Acta Materialia 132 (2017) 276–284

Contents lists available at ScienceDirect

Acta Materialia

journal homepage: www.elsevier.com/locate/actamat

Full length article

Formation of nanometer-sized Cu-Sn-Se particles in $Cu_2ZnSnSe_4$ thin-films and their effect on solar cell efficiency

Torsten Schwarz [a, *], Oana Cojocaru-Mirédin [b], Marina Mousel [c], Alex Redinger [d], Dierk Raabe [a], Pyuck-Pa Choi [e, **]

[a] Max-Planck-Institut für Eisenforschung GmbH, Max-Planck-Straße 1, 40237, Düsseldorf, Germany
[b] RWTH Aachen University, I. Physikalisches Institut IA, 52056, Aachen, Germany
[c] University of Luxembourg, Laboratory for Photovoltaics, 41, Rue du Brill, L-4422, Belvaux, Luxembourg
[d] Helmholtz-Zentrum Berlin, Department Complex Compound Semiconductor Materials for Photovoltaics, 14109, Berlin, Germany
[e] Korea Advanced Institute of Science and Technology, Department of Materials Science and Engineering, 34141, Daejeon, Republic of Korea

ARTICLE INFO

Article history:
Received 22 February 2017
Received in revised form
21 April 2017
Accepted 24 April 2017
Available online 26 April 2017

Keywords:
Atom probe tomography
Microstructure
Precipitates
Transmission electron microscopy
Thin films

ABSTRACT

Atom probe tomography and transmission electron microscopy are used to study the formation of nano-sized Cu-Sn-Se particles in $Cu_2ZnSnSe_4$ thin-films. For a Cu-rich precursor, which was deposited at 320 °C under Cu- and Zn-rich growth conditions, $Cu_{2-x}Se$ grains at the surface are detected. During annealing the precursor at 500 °C in a SnSe + Se atmosphere most of the $Cu_{2-x}Se$ is transformed to $Cu_2ZnSnSe_4$ via the consumption of excessive ZnSe and incorporation of Sn. However, atom probe tomography studies also reveal the formation of various nanometer-sized Cu-Sn-Se particles close to the $CdS/Cu_2ZnSnSe_4$ interface. One of those particles has a composition close to the Cu_2SnSe_3 compound. This phase has a smaller band gap than $Cu_2ZnSnSe_4$ and is proposed to lead to a significant drop in the open-circuit voltage and could be the main cause for a detrimental p-n junction and the zero efficiency of the final device. Possible effects of the other phases on solar cell performance and formation mechanisms are discussed as well.

1. Introduction

The compound semiconductors $Cu_2ZnSn(S,Se)_4$ (CZTS(e)) have recently attracted a great deal of attention as absorber materials for thin-film solar cells [1–4]. As a result of intensive research worldwide, CZTS(e) based solar cells have already achieved 12.6% efficiency [2].

The growth of CZTS(e) films is often hampered by the formation of secondary phases due to the narrow existence regions of CZTS(e) compounds as confirmed by theoretical [5,6] and experimental studies [7,8]. Secondary phases that were observed are predominantly ZnS(e) [9–12], $Cu_xS(e)$ [13,14], $Cu_2SnS(e)_3$ [15,16], and $SnS(e)_x$ [9,14]. In general, they are considered to be detrimental to the cell's performance. $Cu_2SnS(e)_3$, $Cu_2S(e)$ and SnS(e) have smaller band gaps than CZTS(e) and should be avoided by any means as their presence will decrease the open circuit voltage [3]. In agreement with this presumption, CZTS(e) based solar cells with the highest efficiencies are found to be Cu-poor ([Cu]/([Zn]+[Sn]) <1) and Zn-rich ([Zn]/[Sn]>1) [3,17]. Under such growth conditions ZnS(e) can be easily formed. However, ZnS(e) has a larger band gap than CZTS(e) and its detrimental effect on cell efficiency is moderate [3].

Although a Cu-poor and Zn-rich CZTS(e) composition is preferred, an intermediate Cu-rich ([Cu]/([Zn]+[Sn])>1) growth step can be included. For $Cu(In,Ga)Se_2$ it was shown that a Cu-rich ([Cu]/([Ga]+[In])>1) composition for a limited time during the growth process is beneficial for the cell performance due to an increase in grain size and a reduction in recombination activity [18,19]. In a previous work we could demonstrate that the Cu-rich growth step for CZTSe can be easily implemented by using a Cu-rich precursor [20]. The Cu excess leads to the formation of $Cu_{2-x}Se$ at the surface of the Cu-rich precursor, which can be removed by KCN etching. Subsequently, the KCN-treated Cu-rich precursor was annealed in a SnSe + Se atmosphere and led to working cell devices. However, when the $Cu_{2-x}Se$ phase was not removed by KCN etching, the annealed precursor yielded zero efficiency. It was

* Corresponding author.
** Corresponding author.
E-mail addresses: schwarz@mpie.de (T. Schwarz), p.choi@kaist.ac.kr (P.-P. Choi).

http://dx.doi.org/10.1016/j.actamat.2017.04.056
1359-6454/

speculated that this observation is due to the formation of a detrimental Cu-Sn-Se compound during annealing.

Despite these interesting observations, a detailed formation mechanism of the Cu-Sn-Se compound could not be given. In general, there is a lack of knowledge about the formation of Cu-Sn-S(e) compounds during CZTS(e) growth. Direct evidence of the formation of Cu_2SnS_3 was given by Cheng et al. [15]. Using electron dispersive X-ray spectroscopy (EDX) and confocal Raman imaging formation of Cu_2SnS_3 on the surface upon sulfurization of a Zn/Cu/Sn metal stack was detected. This observation was attributed to an incomplete formation of CZTS. Other groups [9,21] used a similar growth procedure and found indications of Cu-Sn-S formation at the CZTS/Mo interface by EDX and X-ray photoelectron spectroscopy. However, it has not yet been clarified whether Cu-Sn-S formation is due to an incomplete sulfurization of the metal stacks or due to decomposition of the CZTS compound at the interface with the Mo back contact [22,23].

Mousel et al. [20] and Wang et al. [24] prepared precursors by a low temperature (320 °C and 110 °C, respectively) co-evaporation process and applied a post-deposition annealing process in a SnSe + Se atmosphere and in a S atmosphere, respectively. Using secondary ion mass spectrometry (SIMS), Mousel et al. [20] detected a Sn-enrichment at the surface of the annealed precursor, which suggested the formation of a Cu-Sn-Se compound, whereas Wang et al. [24] detected Cu-Sn-S compounds at the CZTS/Mo interface by EDX.

However, in most studies direct detection and/or quantification of possibly nano-sized Cu-Sn-Se compounds was too challenging or even impossible due to insufficient spatial resolution of the applied techniques and/or due to the similar structure of e.g. $Cu_2SnS(e)_3$ with CZTS(e) and ZnS(e). To overcome these challenges, we perform complementary atom probe tomography (APT) and scanning transmission electron microscopy (STEM)-EDX measurements in this work. We provided insights into the formation of Cu-Sn-Se particles and the influence of these particles on the overall cell performance.

2. Experimental

2.1. Thin film preparation and device fabrication

The CZTSe films were grown by a sequential process. Two precursors were fabricated in a molecular beam epitaxy system by co-evaporation of Cu, Zn, Sn, and Se onto a Mo-coated soda-lime glass (SLG) substrate at a temperature of 320 °C. Both precursors were grown under Zn-rich ([Zn]/[Sn]>1) conditions. One precursor was Cu-rich ([Cu]/([Zn]+[Sn])>1) and the other one was Cu-poor ([Cu]/([Zn]+[Sn])<1). The absorber films were fabricated by annealing the precursor at 500 °C for 30 min in a SnSe + Se atmosphere. For each of the two precursors one sample was subjected to a 10 wt% KCN etching treatment for 1 min prior to annealing and the other one not. A summary of all samples is given in Table 1.

The samples were etched in a 5 wt% KCN solution for 30 s prior to solar cell finishing. A CdS buffer layer was deposited on the absorber by chemical bath deposition. For current-voltage measurements the samples were finished with magnetron sputtered i-ZnO and Al-doped ZnO layers, and a Ni-Al grid deposited by e-beam evaporation. For more details see Ref. [20].

Table 1
Prepared samples: A and B are precursors (P) and C-F are absorbers with (x) or without (–) KCN etching step prior to annealing. The growth and annealing temperature T for precursor and absorber, respectively, are given as well.

Sample	KCN Etching	T [°C]	Comments
A	–	320	Cu-rich P
B	–	320	Cu-poor P
C	–	500	from Cu-rich P
D	x	500	from Cu-rich P
E	–	500	from Cu-poor P
F	x	500	from Cu-poor P

2.2. Characterization

The overall composition of the Cu-rich and Cu-poor precursor films was measured by EDX at an acceleration voltage of 20 kV in a scanning electron microscope. The preparation of TEM and APT samples was carried out using a dual-beam FIB (FEI Helios Nanolab 600i) according to the lift-out technique described in Ref. [25]. To minimize beam damage due to Ga implantation a low energy (2–5 keV) Ga beam was used. STEM-EDX analyses were performed using a JEOL JEM-2200FS TEM, equipped with a JEOL EX-24063JGT X-ray detector, at an acceleration voltage of 200 kV. Laser-assisted APT analyses were performed using a local electrode atom probe (LEAP™ 3000X HR, Cameca Instruments). Laser pulses of 532 nm wavelength, 12 ps pulse length, 100 kHz pulse frequency, and an energy of 50 pJ were applied at a temperature of 50 K. Additionally, cathodoluminescence (CL) measurements were carried out at liquid nitrogen temperatures using a FEI FIB Helios Nanolab 600, which is equipped with a parabolic mirror, a monochromator (MonoCL4 from Gatan), and a liquid nitrogen cooled photomultiplier tube (R5509-73 from Hamamatsu).

The abovementioned measurements were directly carried out on the CZTSe film for the precursor samples, i.e. before the deposition of CdS, ZnO, and the Ni-Al grid. For the absorber films the measurements were performed after depositing a CdS buffer layer but before the deposition of ZnO and the Ni-Al grid.

3. Results

3.1. Precursor films

In a previous work [20] the present authors detected a Cu-rich surface on the Cu-rich precursor by SIMS depth profiling and found indications for the formation of a Cu-Se phase. However, the distribution of this phase on the sub-micrometer scale was not studied in detail.

STEM-EDX maps shown in Fig. 1a)–d) reveal wedge-shaped regions at the film surface as $Cu_{2-x}Se$ grains as it is also evident from the EDX intensity profile shown in Fig. 1e). The compositions are: 57.6 ± 0.4 at.% Cu and 42.4 ± 1.2 at.% Se for grain 1 (1 in Table 2) and 53.7 ± 0.1 at.% Cu, and 46.3 ± 0.1 at.% Se for the grain 2 (2 in Table 2), respectively. Zn and Sn were not detected for neither of them. Large-scale cross-sectional STEM images (see Fig. S1 in supplementary material) exhibit an inhomogeneous distribution of $Cu_{2-x}Se$ along the surface, i.e. there is no continuous $Cu_{2-x}Se$ layer. Similar observations were made for $CuInS_2$ thin-films by Niki et al. [26]. The Zn-rich regions in Fig. 1c) are a complex ZnSe network which has been discussed in an earlier study [11].

Moreover, we also detect small Cu-rich regions (see Fig. S1 in supplementary material) of rather round shapes more than 500 nm below the surface. Due to their small size and overlap with the surrounding matrix within the ~100–150 nm thick TEM lamella, we could not determine the composition by EDX. However, we detected one $Cu_{2-x}Se$ precipitate in the central cross-sectional absorber region by means of APT [27]. The composition of this precipitate is 52.6 ± 1.2 at.% Cu, 2.0 ± 0.4 at.% Zn, 1.8 ± 0.3 at.% Sn, and 43.6 ± 1.2 at.% Se (6 in Table 2). Thus, it is doped with Zn and Sn to some extent. The compositions of the detected $Cu_{2-x}Se$ particles vary as shown in Table 2. It is revealed that some grains are doped with Zn and Sn and some are not. Besides $Cu_{2-x}Se$ and ZnSe, we

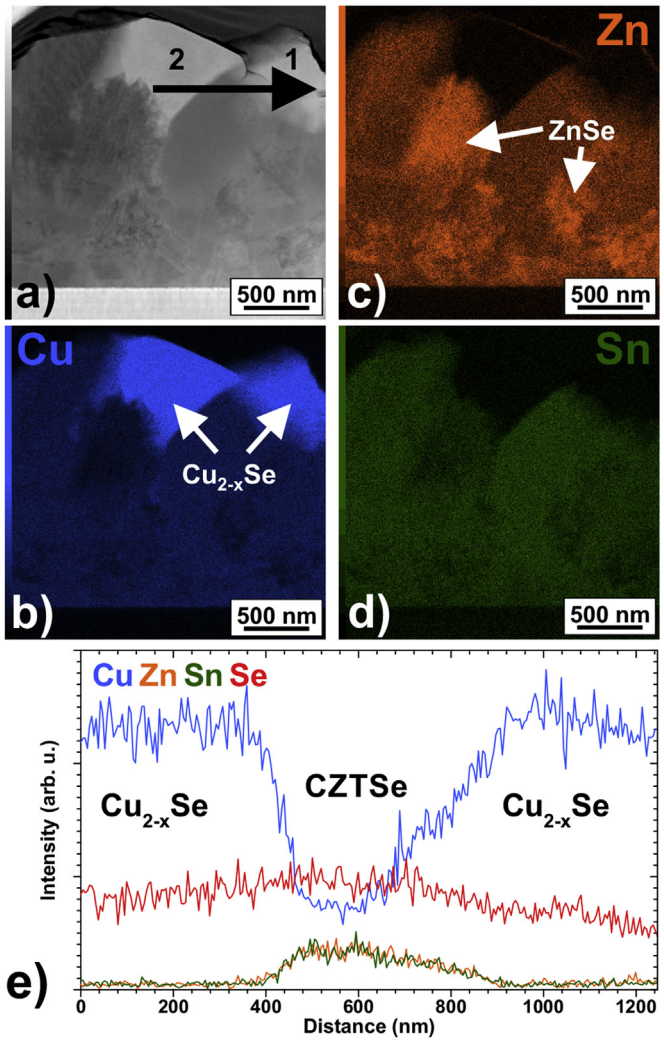

Fig. 1. a)-d) STEM-EDX measurement of a cross-section from the Cu-rich precursor. a) STEM dark field (DF) image, b) distribution of Cu-K (blue), c) of Zn-K (orange), and d) of Sn-L (dark green). e) EDX intensity profile along the arrow shown in a). (For interpretation of the references to colour in this figure legend, the reader is referred to the web version of this article.)

Table 2
Chemical composition of different Cu-Se and Cu-Sn-Se grains measured by STEM-EDX and APT. The errors given for APT measurements are 2σ standard deviations resulting from the sampling volumes. Reproduced with permission. [29] © 2015 Shaker-Verlag GmbH Aachen.

Number	Cu [at.%]	Zn [at.%]	Sn [at.%]	Se [at.%]	Sample	Method
1	57.6 ± 0.4	–	–	42.4 ± 1.2	A	STEM-EDX
2	53.7 ± 0.1	–	–	46.3 ± 0.1	A	STEM-EDX
3	53.8 ± 0.1	–	–	46.2 ± 0.2	A	STEM-EDX
4	55.0 ± 0.4	0.8 ± 0.2	–	44.1 ± 1.0	A	STEM-EDX
5	55.7 ± 0.4	–	–	43.9 ± 1.0	A	STEM-EDX
6	52.6 ± 1.2	2.0 ± 0.4	1.8 ± 0.3	43.6 ± 1.2	A	APT
7	48.9 ± 0.4	0.3 ± 0.04	7.8 ± 0.2	40.3 ± 0.4	A	APT
8	65.6 ± 0.8	0.0	0.0	34.4 ± 0.8	A	APT
9	47.7 ± 0.2	0.9 ± 0.04	10.5 ± 0.1	41.0 ± 0.2	C	APT
10	46.1 ± 0.7	0.8 ± 0.1	9.2 ± 0.4	43.9 ± 0.7	C	APT
11	34 ± 2	4 ± 0.5	12 ± 1	51 ± 1	C	APT

observed another secondary phase. In an APT measurement acquired from a region ~350 nm above the Mo back contact, as shown in Fig. 2 we detected a ~10 nm thick region, which contains a relatively high concentration of Sn with 7.8 at.% and only 0.3 at.% Zn (7 in Table 2). The corresponding proximity histogram (proxigram: profile against proximity to an interface of arbitrary geometry [28]) in Fig. 2e) across the CZTSe/Cu-Sn-Se interface marked by the 30 at.% Cu iso-concentration surface reveals a depletion of Cu and a pile-up of Zn on the CZTSe side. The discrepancy between the ~6 at.% Zn in the Cu-Sn-Se region shown in the proxigram and the calculated Zn concentration of 0.3 at.% is due to a strong overlap of ^{63}Cu and ^{65}Cu peaks with ^{64}Zn and ^{66}Zn peaks (for more details see the supplementary material). This overlap leads to an overestimation of the Zn concentration in the proxigram. However, it can be corrected by a peak deconvolution algorithm (included in the commercial software IVAS 3.6.6, Cameca Instruments) for the calculated compositions given in Table 2. Although a low voltage (5 kV) was applied during the final FIB preparation step, a Ga enrichment of up to 7.5 at.% directly at the CZTSe/Cu-Sn-Se interface was detected. The penetration depth of Ga seems to be higher in Cu-(Sn)-Se than in CZTSe.

The proxigram also reveals a Na concentration of ~2.5 at.% in the Cu-Sn-Se grain, as it is also apparent from the Na distribution map shown in Fig. 2d). The detection of Na in the precursor film indicates that Na atoms already start to diffuse at 320 °C from the SLG substrate through the Mo layer into the CZTSe film. Furthermore, Na is enriched at the apex of the APT specimen in a very thin layer

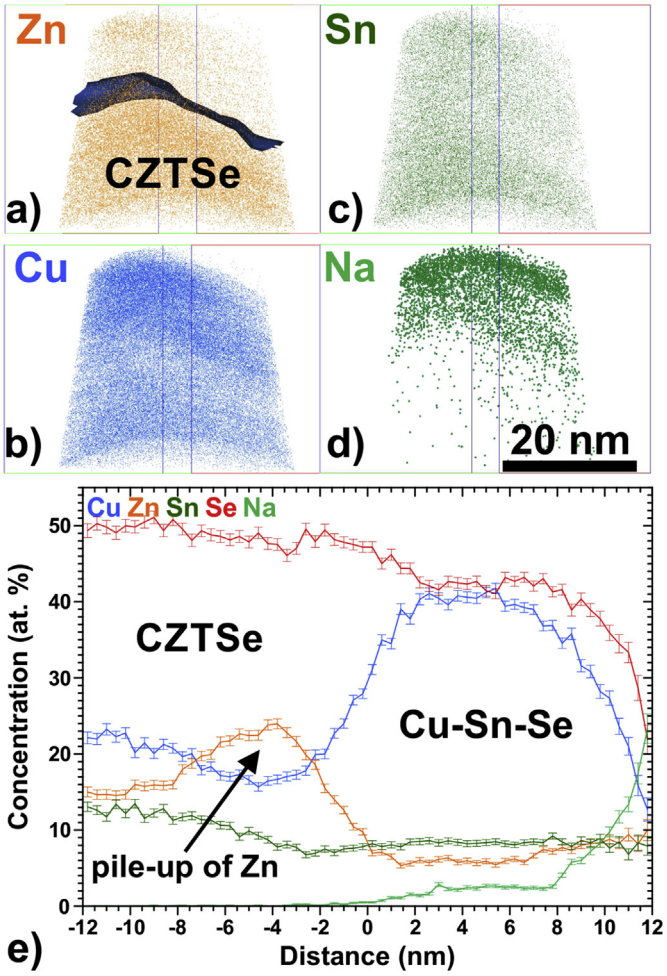

Fig. 2. a)-d) APT elemental maps of Zn (orange), Cu (blue), Sn (dark green), and Na (green) acquired from the Cu-rich precursor. The apex of the APT sample was ~350 nm above the Mo back contact. e) Proxigram across the 30 at.% Cu iso-concentration surface (blue) shown in a). (For interpretation of the references to colour in this figure legend, the reader is referred to the web version of this article.)

(<5 nm in thickness), where the Na concentration is approximately ten times higher than in the Cu-Sn-Se region (see supplementary material for details).

For the Cu-poor precursor we also detected a complex ZnSe network throughout the film due to Zn-rich growth conditions (see Fig. S2 in supplementary material). However, $Cu_{2-x}Se$ and Cu-Sn-Se compounds cannot be detected due to Cu-poor growth conditions. Furthermore, the Cu-poor precursor exhibits small grains with a size of only a few 100 nm, whereas the Cu-rich precursor has grains larger than 1 μm (cf. Fig. S1 in supplementary material).

Fig. 3a) shows a panchromatic CL image from the surface of the Cu-rich precursor. There is almost no light emission detectable although a high injection with a beam current of 22 nA was used. Only a few grains (bright contrast) emit light. In contrast, for the Cu-poor precursor we detected light from all grains (see Fig. 3b)) at a beam current as low as 1.4 nA.

3.2. Absorber films

The annealed Cu-rich precursor (final absorber) without KCN etching prior to annealing yields no working device. Mousel et al. [20] attributed this observation to the Cu-rich nature of the precursor. It was shown that due to the incorporation of Sn the overall composition (measured by EDX) shifts from Cu-rich to Cu-poor. It was expected that the $Cu_{2-x}Se$ grains form a Cu-Sn-Se phase on the surface during annealing in a SnSe + Se atmosphere. However, direct evidence was not provided [20].

Indeed, representative STEM-EDX measurements from the absorber cross-section shown in Fig. 4a)–d)) confirm that there is no longer $Cu_{2-x}Se$ present throughout the absorber. Instead, we detect only ZnSe. Nevertheless, STEM-EDX measurements do not reveal the formation of any Cu-Sn-Se phase on the micro-scale. This observation is also true for the surface region where its presence was expected due to the $Cu_{2-x}Se$ grains in the Cu-rich precursor, which were up to several 100 nm in size. However, by using APT we could detect nano-sized particles of a Cu-Sn-Se phase 200 nm below the absorber surface. Cu-Sn-Se particles were not detected deeper inside the absorber or at the Mo back contact. One APT dataset is shown in Fig. 5. One can find a clear Cu enrichment and Zn depletion at the top of the tip (region 9). Furthermore, a pile-up of Zn and a slight Cu depletion can be found on the CZTSe side in the proxigram across the CZTSe/Cu-Sn-Se interface (blue), which is marked by the 30 at.% Cu iso-concentration surface in Fig. 5c). The same observation was made for Cu and Zn at a CZTSe/Cu-Sn-Se interface in the precursor film (cf. Fig. 2). As for the precursor there is a strong contribution of Cu peaks to Zn peaks, which leads to a high Zn concentration in the Cu-Sn-Se region in the proxigram (see supplementary material). The calculated composition of the Cu-Sn-Se region is 47.7 ± 0.2 at.% Cu, 0.9 ± 0.04 at.% Zn, 10.5 ± 0.1 at.% Sn, and 41.0 ± 0.2 at.% Se (9 in Table 2). Thus, the Cu-Sn-Se phase is Zn doped. The compositions of all Cu-Sn-Se regions found by APT from the identical absorber are summarized in Table 2.

The annealed Cu-rich precursor with prior KCN etching exhibits only ZnSe as secondary phase due to the removal of $Cu_{2-x}Se$ at the precursor surface [20]. Hence, the overall composition measured by EDX after annealing remains the same, i.e. there is no incorporation of Sn and no formation of Cu-Sn-Se phases [20]. The same results are obtained for the annealed Cu-poor precursors. Due to the absence of $Cu_{2-x}Se$ there is no change in composition after annealing irrespective of whether the precursor was etched in KCN solution or not [20]. ZnSe is the only detected secondary phase in those absorber films. Latter three absorber films lead to working solar cells (see Table 3 and discussion part).

Fig. 3c) shows a representative comparison of the CL spectra obtained from the annealed Cu-rich precursor with (solid line) and without (dashed line) KCN etching step. Both CL spectra reveal a

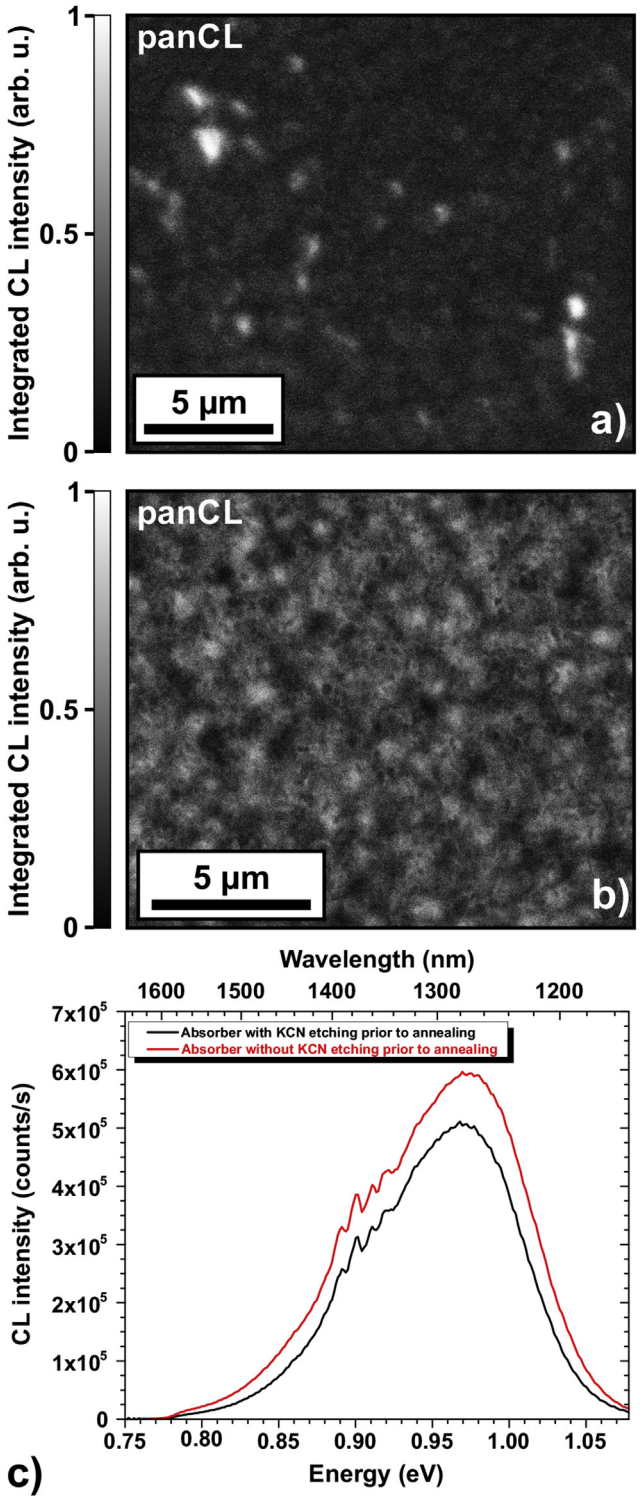

Fig. 3. a)-b) Panchromatic CL image of the Cu-rich and Cu-poor precursor acquired at 81 K, at an acceleration voltage of 10 kV, and at a beam current of 22 nA and 1.4 nA, respectively. c) Comparison between CL spectra of the absorber with (black solid line) and without (red dashed line) KCN etching prior to annealing of the Cu-rich precursor. CL spectra were acquired at 81 K, at an acceleration voltage of 10 kV, at a beam current of 11 nA, and were corrected for the detector and grating response. (For interpretation of the references to colour in this figure legend, the reader is referred to the web version of this article.)

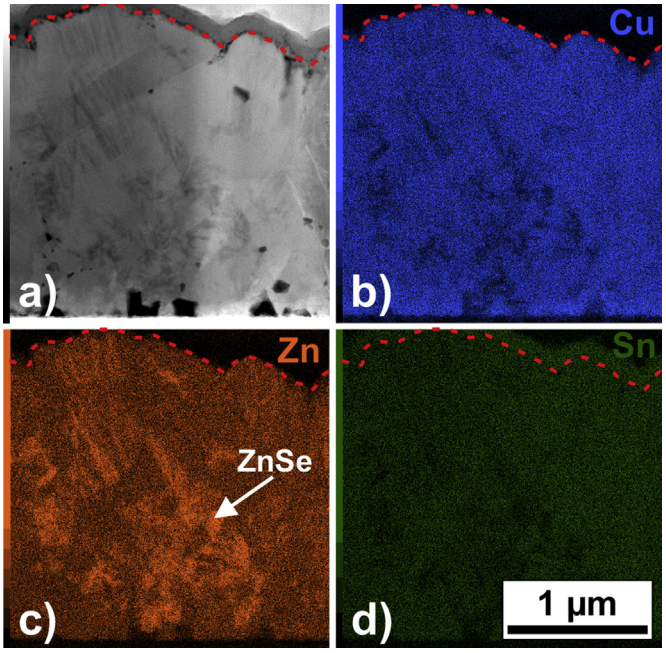

Fig. 4. a)-d) STEM-EDX measurement of a cross-section from the annealed Cu-rich precursor (final absorber). a) STEM DF image, b) distribution of Cu-K (blue), c) of Zn-K (orange), and d) of Sn-L (dark green). The dashed line (red) marks the CdS/CZTSe interface. Due to overlapping Sn-L and Cd-L lines there seems to be a Sn-enrichment in the CdS buffer. (For interpretation of the references to colour in this figure legend, the reader is referred to the web version of this article.)

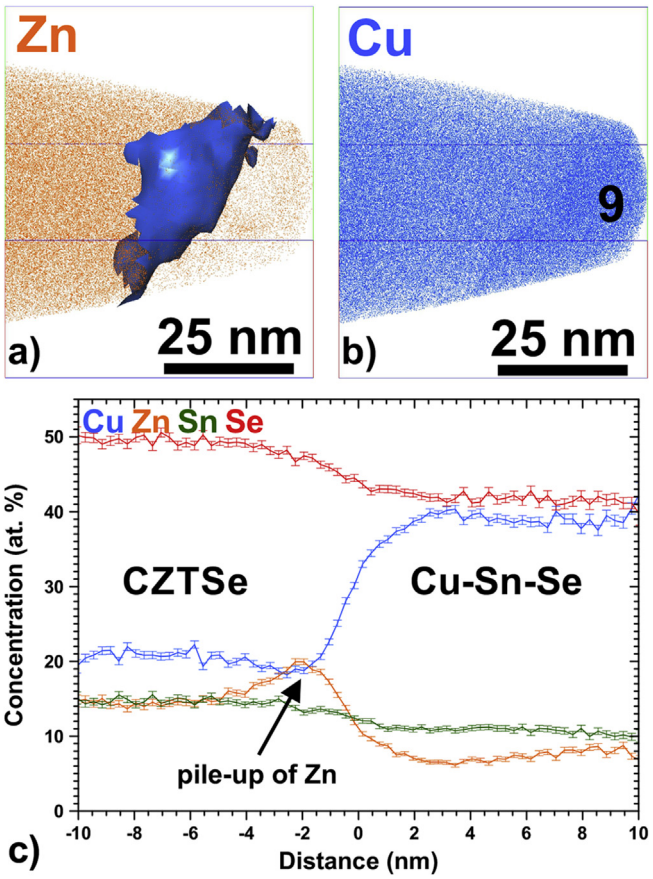

Fig. 5. a) and b) APT elemental maps of Zn (orange) and Cu (blue) acquired from the annealed Cu-rich precursor without KCN etching prior to annealing. The apex of the APT is ~200 nm below the CZTSe film surface. e) Proxigram across the 30 at.% Cu iso-concentration surface (blue) shown in a). (For interpretation of the references to colour in this figure legend, the reader is referred to the web version of this article.)

similar spectrum shape and yield, which was confirmed at other randomly chosen positions of both samples. In general, the CL yield of the absorber films is two and three orders of magnitudes higher than for the Cu-poor and Cu-rich precursor, respectively. The much lower CL yield of the precursor films compared to the final absorber could be due to a higher density of detrimental defects acting as non-radiative recombination centers (see also discussion). Absorber films prepared from the Cu-poor precursor show a similar CL yield as the absorber films made from the Cu-rich precursor, which is discussed elsewhere [29].

4. Discussion

4.1. Formation of secondary phases

In this part we focus on the development of a growth model, which we suggest for the formation of secondary phases in the Cu-rich precursor and the annealed Cu-rich precursor without prior KCN etching. The other samples only contain ZnSe as secondary phase and its formation mechanism is similar to the ZnSe formation in the Cu-rich precursor.

Besides CZTSe, several secondary phases are formed in the Cu-rich precursor film due to the Cu-rich and Zn-rich growth. After an initial growth of small (~few 100 nm) CZTSe grains excess Cu and Se atoms, which cannot be incorporated into the CZTSe grains, diffuse on the surface until $Cu_{2-x}Se$ particles are nucleated, which grow and partly cover the film surface. Since the Cu diffusivity is large enough, also excess Cu atoms in CZTSe grains can diffuse towards the film surface and form $Cu_{2-x}Se$ grains [30]. This assumption is supported by the finding that the composition of single CZTSe grains of the Cu-rich precursor is Cu-poor [31]. Hence, the formation energy of V_{Cu} vacancies is decreased compared to stoichiometric CZTSe leading to a high population of these defects [6,17,32] and the diffusion of Cu can take place via V_{Cu} vacancies. In parallel, excess Cu and Se may cover the CZTSe surface by a few monolayer thin film of Cu-Se, similar to the work of Niki et al. [26]. During further growth Cu, Zn, Sn, and Se atoms condensate on the $Cu_{2-x}Se$ grains and the thin Cu-Se film surface and are absorbed. After absorption they diffuse towards the Cu-Se/CZTSe interface and are incorporated into the growing CZTSe grains. In contrast to Cu, the Zn diffusivity is low [30] and, therefore, the excess Zn atoms form ZnSe which is randomly distributed across the precursor film. These findings are schematically summarized in Fig. 6a) and b)). For the Cu-poor precursor such a Cu-Se film does not cover CZTSe grains, which aids the grain growth. A possible reason for the unaided grain growth might be smaller sticking coefficients of the single elements on a CZTSe surface compared to Cu-Se which in turn leads to a higher desorption rate. Thus, the growth of CZTSe is impeded.

Some $Cu_{2-x}Se$ grains of the Cu-rich precursor are doped to some extent with Zn and Sn, while the Cu-Sn-Se phases are doped with Zn. The solubility of Zn in $Cu_{2-x}Se$ and Cu-Sn-Se seems to be very small. Thus, excess Zn atoms cannot be incorporated to form CZTSe and lead to a pile-up of Zn on the CZTSe side at the interface between CZTSe and $Cu_{2-x}Se$ or Cu-Sn-Se, respectively. This assertion is supported by the fact that detected ZnSe is surrounded by CZTSe or it is located at the interface of adjacent $Cu_{2-x}Se$ grains (cf. Fig. 1). However, ZnSe itself cannot be found in those $Cu_{2-x}Se$ grains (see Fig. S1 in supplementary material).

The formation of Cu-Sn-Se phases can already occur during the precursor growth process via the incorporation of Sn into Cu-Se

Table 3
List of solar cell parameters under illumination for the samples given in Table 1. The parameters are averaged over six solar cells (single parameters are listed in Ref. [20]). η is the efficiency, V_{OC} the open circuit voltage, J_{SC} the short-circuit current density, FF the fill factor, R_S the series resistance, G_{SH} the shunt conductance, A the diode factor, and J_0 the saturation current density. Reproduced with permission. [20] Copyright © 2013 WILEY-VCH Verlag GmbH & Co. KGaA, Weinheim

Sample	η [%]	V_{OC} [mV]	J_{SC} [mA/cm^2]	FF [%]	R_S [Ωcm^2]	G_{SH} [mS/cm^2]	A	J_0 [mA/cm^2]
C	0	–	–	–	–	–	–	–
D	6.0	348	30.9	56	0.48	5.3	2.20	7.6×10^{-2}
E	3.4	284	24.7	42	0.50	18.4	2.62	3.9×10^{-1}
F	4.8	338	26.7	53	0.48	9.2	2.03	5.4×10^{-2}

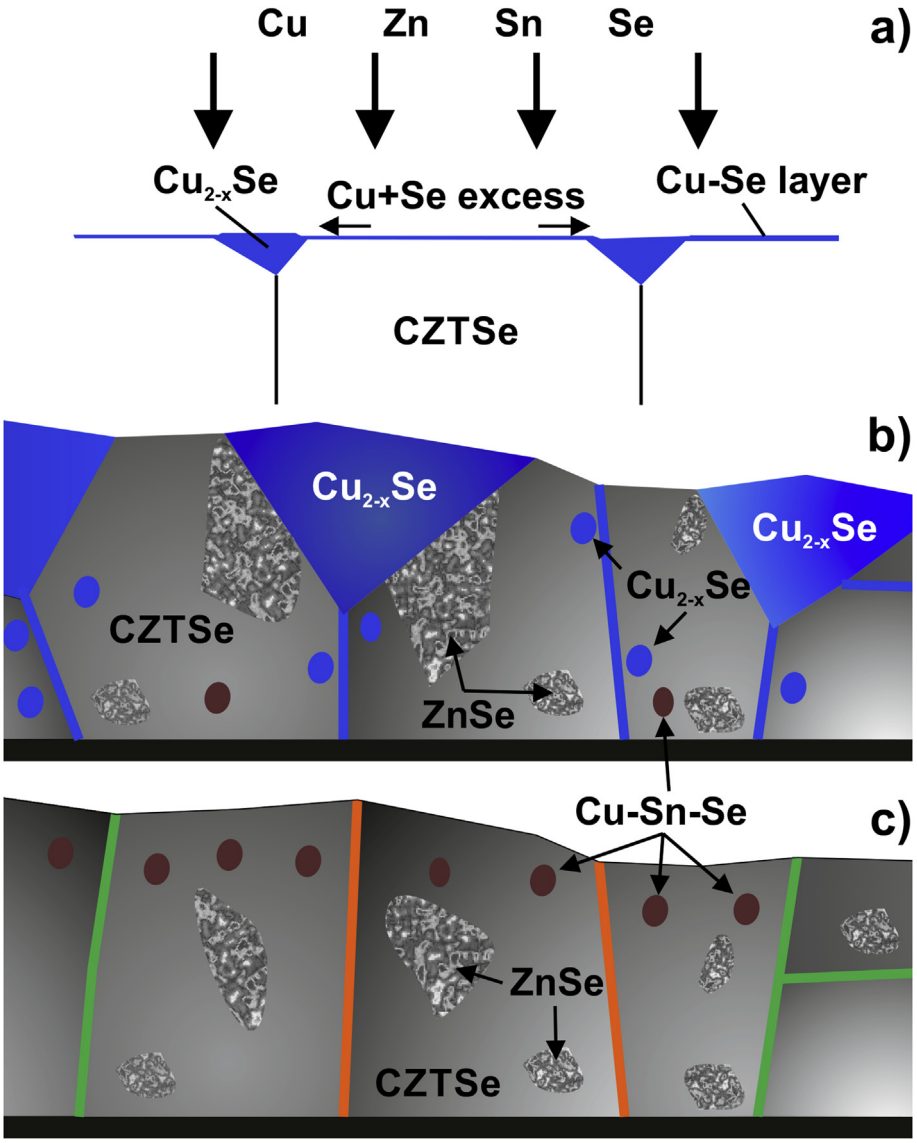

Fig. 6. a) Growth model of CZTSe grains under Cu-rich conditions in the presence of $Cu_{2-x}Se$ grains and a thin Cu-Se layer. b) Schematic drawing of the Cu-rich precursor. The blue lines represent Cu-enriched CZTSe GBs. c) Schematic drawing of Cu-Sn-Se distribution after annealing the Cu-rich precursor in a SnSe + Se atmosphere without prior KCN etching. The orange and green lines represent Zn-enriched and Na/K-decorated CZTSe GBs, respectively. (For interpretation of the references to colour in this figure legend, the reader is referred to the web version of this article.)

phases. This finding is actually expected for the annealed precursor. On the one hand, taking only the Cu, Sn, and Se concentration for region 7 in Table 2 into account, a composition of ~$Cu_{6.3}SnSe_{5.2}$ is measured. This composition is similar to the known Cu_5SnS_4 phase [33], which has not yet been detected in CZTS(e) thin-films. On the other hand, the formation of Cu_2SnSe_3 is kinetically limited due to an insufficient incorporation of Sn and, therefore, the detected $Cu_{6.3}SnSe_{5.2}$ compound may be metastable and in a transition state to it. However, we cannot exclude the formation of Cu_2SnSe_3 in the precursor film.

Annealing of the precursor film in a SnSe + Se atmosphere at 500 °C shifts the overall composition (measured by EDX) from the previously Cu-rich side to the Cu-poor one in the phase diagram due to the incorporation of Sn into the absorber film. Sn is

incorporated to form CZTSe via the consumption of $Cu_{2-x}Se$ at the surface and of ZnSe, which is in the close vicinity of $Cu_{2-x}Se$. A possible reaction path is:

$$Cu_2Se(s) + ZnSe(s) + SnSe_2(g) \Leftrightarrow Cu_2ZnSnSe_4(s) \quad (1)$$

In order to simplify this reaction, Cu_2Se is used instead of $Cu_{2-x}Se$.

The smaller $Cu_{2-x}Se$ and Cu-Sn-Se grains, which are predominantly detected in the absorber center of the Cu-rich precursor, will be consumed during annealing. Both compounds are either directly incorporated into CZTSe grains or they form CZTSe by concurrent consumption of neighboring ZnSe. The required Sn for this formation may stem from the already present CZTSe grains. The corresponding reaction paths are:

$$a \cdot Cu_2Se(s) + b \cdot ZnSe(s) + c \cdot Cu_2ZnSnSe_4(s) \Leftrightarrow Cu_2ZnSnSe_4(s), \quad (2a)$$

and

$$a \cdot Cu - Sn - Se(s) + b \cdot ZnSe(s) \Leftrightarrow Cu_2ZnSnSe_4(s). \quad (2b)$$

The letters *a*, *b*, and *c* denote the corresponding mole fractions. CZTSe probably does not decompose due to the incorporation of $Cu_{2-x}Se$ and Cu-Sn-Se grains or consumption of Sn because its volume fraction is significantly larger than that of $Cu_{2-x}Se$ and Cu-Sn-Se.

Besides CZTSe, nanometer-sized Cu_2SnSe_3 and other Cu-Sn-Se particles will be formed due to the incorporation of Sn from the SnSe + Se atmosphere into a small fraction of the $Cu_{2-x}Se$ grains on the absorber surface. Due to the fact that most of the $Cu_{2-x}Se$ grains are consumed to form CZTSe and only a small fraction to form nanometer-sized Cu-Sn-Se compounds, we do not observe latter in STEM-EDX measurements. This finding is schematically shown in Fig. 6c). Taking only the Cu, Sn, and Se concentration into account the composition of region 9 and 10 (see Table 2) can be rewritten as $Cu_{4.5}SnSe_{3.9}$ and $Cu_{5.0}SnSe_{4.8}$. These compositions are also close to Cu_5SnSe_4. In contrast, the measured composition of region 11 can be probably assigned to the detrimental secondary phase Cu_2SnSe_3. However, all three Cu-Sn-Se compounds have a higher Zn concentration than the Cu-Sn-Se compound of the precursor.

4.2. Effect on cell efficiency

The direct use of the precursor films as an absorber film yields no working solar cells [20], where the reasons are manifold. Possible reasons are recombination losses due to a high defect density and recombination at ZnSe/CZTSe interfaces, which limits the open-circuit voltage V_{oc}. Furthermore, we detected Cu-enriched CZTSe grain boundaries (GB), which are probably not electrically benign [31]. Moreover, due to the low growth temperature inclusions of stannite structured CZTSe may be present in the kesterite structured matrix. We cannot distinguish these two phases from each other by X-ray diffraction because Cu^+ and Zn^{2+} are isoelectronic. Due to the smaller band gap of stannite compared to kesterite the cell efficiency can be further reduced [1]. In addition, the $Cu_{2-x}Se$ phase, which is detected in the Cu-rich precursor at the surface up to the film middle and at Cu-enriched CZTSe GBs [31], is highly conductive [26]. It can lead to shunt paths and, therefore, to shunting of the final device. Moreover, the detected Cu-Sn-Se phases in the Cu-rich precursor film can have a smaller band gap than CZTSe. Hence, they may act as traps for electrons and holes and thus as recombination centers, reducing the V_{oc} [34].

In order to obtain a working solar cell for the samples studied in this work, it is necessary to anneal the precursor [20]. As presented in Table 3 absorbers prepared from the Cu-poor precursor lead to working devices. The higher efficiency of the KCN treated sample F compared to the untreated sample E is due to the KCN etching, e.g. by cleaning the surface. In contrast, final absorbers prepared from the Cu-rich precursor only lead to working devices if a KCN etching step was applied prior to annealing. Here, only the KCN treated sample D yields a working solar cell with 6% efficiency.

The question arises why sample C fails. There is no $Cu_{2-x}Se$ present in the annealed absorber film, which can lead to shunt paths like in the Cu-rich precursor. Furthermore, in contrast to the CZTSe GB composition in the precursor the CZTSe GBs in the final absorber show either a slight Cu depletion or they are decorated by Na and K, which may render them electrically inactive [31]. Although we detect a complex ZnSe network in sample C similar to the Cu-rich precursor, which can lead to recombination losses, it cannot solely explain the failure because we detect ZnSe in working devices as well [11]. Another possible cause might be a high density of detrimental deep defects or dislocations acting as non-radiative recombination centers. For example, a possible incorporation of Sn during annealing into the Cu-poor CZTSe grains may promote the formation of Sn related deep defects such as Sn_{Cu} and Sn_{Zn} antisites [17]. However, we can also exclude this as the main reason. Comparison between CL spectra of absorber films made from the same Cu-rich precursor with and without KCN etching prior to annealing reveals that they have almost the same spectrum shape and CL yield close to the band gap. The latter one indicates that the defect concentration in both absorbers are similar, independent of which defect is dominant or whether it is a deep defect or not. In contrast to the absorbers, there is almost no CL yield of the Cu-rich precursor film, i.e. during annealing annihilation of detrimental defects takes place.

Hence, there must be another shunt path and/or efficient recombination path in sample C. The only difference, which we can detect in our measurements, between sample C and the other absorber samples is the presence of Cu-Sn-Se compounds as secondary phase in the absorber layer. Since sample C shows no diode behavior (see current-voltages curves in supplementary material), one could assume that a shunt path created by highly conductive Cu-Sn-Se phases located at CZTSe grain boundaries might be the reason for the failure of sample C. However, Cu-Sn-Se phases were neither detected in the bulk throughout the entire absorber depth nor close to CZTSe grain boundaries. Furthermore, the CZTSe grain boundaries in sample C exhibit no detrimental Cu enrichment as in the Cu-rich precursor [31].

Hence, we propose that recombination related to Cu-Sn-Se phases via deep defects mainly causes the failure of sample C. One of the Cu-Sn-Se compounds is Cu_2SnSe_3 with a narrow band gap of $E_g \approx 0.4–0.8$ eV [35–37], which is smaller than that of CZTSe ($E_g = 1.0$ eV) [3]. The band gap of the Cu-Sn-Se compound having a composition close to Cu_6SnSe_5 is not known. However, its band gap may be also smaller than that of CZTSe. Moreover, from the present study we do not gain insights into the doping of the Cu-Sn-Se phases. It could well be that the doping is too high which would also promote recombination. Band offsets between the CZTSe matrix and the Cu-Sn-Se compounds might also be unfavorable. The APT tips containing these phases were prepared less than 200 nm below the surface, i.e. they are present in the space charge region, where recombination can be very effective [38]. In general, a significantly lower CL yield would be expected independent of whether the recombination is radiative or non-radiative. However, in CL electron-hole pairs are not only generated close to Cu-Sn-Se particles. The generation volume at 10 keV acceleration voltage can be a few hundred nanometer in size [39], i.e. also in the surrounding CZTSe grains electron-hole pairs are generated, which explains the similar CL yield of sample C and D (cf. Fig. 3c)).

Whether recombination related to Cu-Sn-Se compounds with $E_g < 0.8$ eV is radiative or not, we cannot determine since our CL setup has a cut-off of the detector around ~0.75–0.80 eV.

Furthermore, Cu-Sn-Se compounds, which may have a larger band gap compared to CZTSe, can also lead to recombination at the Cu-Sn-Se/CZTSe interface or act as barriers for both holes and electrons depending on the phase, in which they are generated.

Therefore, the nanometer-sized Cu-Sn-Se particles can lead to a high reverse saturation current and to a reduction of the open-circuit voltage. In conclusion, the detected Cu-Sn-Se particles might be a main origin for a bad p-n junction and could explain the zero cell efficiency of the final device.

5. Conclusions

We conducted APT and STEM-EDX measurements to study the formation of Cu-Sn-Se compounds and their effect on cell performance. We detected $Cu_{2-x}Se$ grains mainly at the surface of the co-evaporated Cu-rich precursor due to Cu-rich growth conditions. Some of them are doped with Zn and Sn. The Sn incorporation can be as high that Cu-Sn-Se compounds are already formed in the precursor. The incorporation of Sn from the SnSe + Se atmosphere during annealing without prior KCN etching of the Cu-rich precursor leads mainly to the formation of CZTSe via the consumption of Cu_{2-x} and ZnSe. However, we could also show that nanometer-sized Cu-Sn-Se particles such as Cu_2SnSe_3 are formed close to the CdS/CZTSe interface. Cu-Sn-Se compounds having a smaller band gap compared to CZTSe, e.g. Cu_2SnSe_3, can act as a very efficient recombination center. Hence, Cu-Sn-Se phases might be a main origin for bad p-n junction and the zero efficiency of the final device.

Acknowledgements

The authors thank Susanne Siebentritt from the University of Luxembourg as well as Baptiste Gault from Max-Planck-Institut für Eisenforschung GmbH for fruitful discussions. Furthermore, the authors are grateful to Uwe Tezins and Andreas Sturm for their support to the APT and FIB facilities at Max-Planck-Institut für Eisenforschung GmbH. This work was funded by the German Research Foundation (DFG) (Contract CH 943/2-1 and GA 2450/1-1), and by the Luxembourgish Fonds National de la Recherche. Alex Redinger acknowledges financial support from the Fonds national de la recherche, project number 7842175.

Appendix A. Supplementary data

Supplementary data related to this article can be found at http://dx.doi.org/10.1016/j.actamat.2017.04.056.

References

[1] S. Siebentritt, S. Schorr, Kesterites - a challenging material for solar cells, Prog. Photovoltaics 20 (5) (2012) 512–519.
[2] W. Wang, M.T. Winkler, O. Gunawan, T. Gokmen, T.K. Todorov, Y. Zhu, D.B. Mitzi, Device characteristics of CZTSSe thin-film solar cells with 12.6% efficiency, Adv. Energy Mater. 4 (7) (2014) 1301465.
[3] S. Siebentritt, Why are kesterite solar cells not 20% efficient? Thin Solid Films 535 (2013) 1–4.
[4] G. Brammertz, M. Buffière, S. Oueslati, H. ElAnzeery, K. Ben Messaoud, S. Sahayaraj, C. Köble, M. Meuris, J. Poortmans, Characterization of defects in 9.7% efficient Cu2ZnSnSe4-CdS-ZnO solar cells, Appl. Phys. Lett. 103 (163904) (2013).
[5] A. Walsh, S. Chen, S.-H. Wei, X.-G. Gong, Kesterite Thin-film solar cells: advances in materials modelling of Cu2ZnSnS4, Adv. Energy Mater. 2 (4) (2012) 400–409.
[6] T. Maeda, S. Nakamura, T. Wada, First-principles calculations of vacancy formation in In-free photovoltaic semiconductor Cu2ZnSnSe4, Thin Solid Films 519 (21) (2011) 7513–7516.
[7] I.V. Dudchak, L.V. Piskach, Phase equilibria in the Cu2SnSe3–SnSe2–ZnSe system, J. Alloys Compd. 351 (1–2) (2003) 145–150.
[8] I.D. Olekseyuk, I.V. Dudchak, L.V. Piskach, Phase equilibria in the Cu2S–ZnS–SnS2 system, J. Alloys Compd. 368 (1–2) (2004) 135–143.
[9] C. Platzer-Bjorkman, J. Scragg, H. Flammersberger, T. Kubart, M. Edoff, Influence of precursor sulfur content on film formation and compositional changes in Cu2ZnSnS4 films and solar cells, Sol. Energ Mat. Sol. C 98 (2012) 110–117.
[10] A. Redinger, K. Hones, X. Fontane, V. Izquierdo-Roca, E. Saucedo, N. Valle, A. Perez-Rodriguez, S. Siebentritt, Detection of a ZnSe secondary phase in coevaporated Cu2ZnSnSe4 thin films, Appl. Phys. Lett. 98 (10) (2011) 101907.
[11] T. Schwarz, O. Cojocaru-Miredin, P. Choi, M. Mousel, A. Redinger, S. Siebentritt, D. Raabe, Atom probe study of Cu2ZnSnSe4 thin-films prepared by co-evaporation and post-deposition annealing, Appl. Phys. Lett. 102 (4) (2013) 042101.
[12] J.T. Wätjen, J. Engman, M. Edoff, C. Platzer-BjÖrkman, Direct evidence of current blocking by ZnSe in Cu2ZnSnSe4 solar cells, Appl. Phys. Lett. 100 (17) (2012) 173510.
[13] G.S. Babu, Y.B.K. Kumar, P.U. Bhaskar, S.R. Vanjari, Effect of Cu/(Zn plus Sn) ratio on the properties of co-evaporated Cu2ZnSnSe4 thin films, Sol. Energ Mat. Sol. C 94 (2) (2010) 221–226.
[14] R.A. Wibowo, W.S. Kim, E.S. Lee, B. Munir, K.H. Kim, Single step preparation of quaternary Cu2ZnSnSe4 thin films by RF magnetron sputtering from binary chalcogenide targets, J. Phys. Chem. Solids 68 (10) (2007) 1908–1913.
[15] A.J. Cheng, M. Manno, A. Khare, C. Leighton, S.A. Campbell, E.S. Aydil, Imaging and phase identification of Cu2ZnSnS4 thin films using confocal Raman spectroscopy, J. Vac. Sci. Technol. A 29 (5) (2011) 051203.
[16] M. Mousel, A. Redinger, R. Djemour, M. Arasimowicz, N. Valle, P. Dale, S. Siebentritt, HCl and Br-2-MeOH etching of Cu2ZnSnSe4 polycrystalline absorbers, Thin Solid Films 535 (2013) 83–87.
[17] S. Chen, A. Walsh, X.G. Gong, S.H. Wei, Classification of lattice defects in the kesterite Cu2ZnSnS4 and Cu2ZnSnSe4 earth-abundant solar cell absorbers, Adv. Mater 25 (11) (2013) 1522–1539.
[18] J.K. Larsen, L. Gutay, S. Siebentritt, Influence of secondary phase CuxSe on the optoelectronic quality of chalcopyrite thin films, Appl. Phys. Lett. 98 (201910) (2011).
[19] I. Repins, C. Beall, N. Vora, C. DeHart, D. Kuciauskas, P. Dippo, B. To, J. Mann, W.C. Hsu, A. Goodrich, R. Noufi, Co-evaporated Cu2ZnSnSe4 films and devices, Sol. Energ Mat. Sol. C 101 (2012) 154–159.
[20] M. Mousel, T. Schwarz, R. Djemour, T.P. Weiss, J. Sendler, J.C. Malaquias, A. Redinger, O. Cojocaru-Miredin, P.P. Choi, S. Siebentritt, Cu-Rich precursors improve kesterite solar cells, Adv. Energy Mater. 4 (2) (2014) 1300543.
[21] A. Ennaoui, M. Lux-Steiner, A. Weber, D. Abou-Ras, I. Kotschau, H.W. Schock, R. Schurr, A. Holzing, S. Jost, R. Hock, T. Voss, J. Schulze, A. Kirbs, Cu2ZnSnS4 thin film solar cells from electroplated precursors: Novel low-cost perspective, Thin Solid Films 517 (7) (2009) 2511–2514.
[22] J.J. Scragg, J.T. Wätjen, M. Edoff, T. Ericson, T. Kubart, C. Platzer-Björkman, A detrimental reaction at the molybdenum back contact in Cu2ZnSn(S,Se)4 thin-film solar cells, J. Am. Chem. Soc. 134 (47) (2012) 19330–19333.
[23] J.J. Scragg, P.J. Dale, D. Colombara, L.M. Peter, Thermodynamic aspects of the synthesis of thin-film materials for solar cells, Chemphyschem a Eur. J. Chem. Phys. Phys. Chem. 13 (12) (2012) 3035–3046.
[24] K. Wang, B. Shin, K.B. Reuter, T. Todorov, D.B. Mitzi, S. Guha, Structural and elemental characterization of high efficiency Cu2ZnSnS4 solar cells, Appl. Phys. Lett. 98 (051912) (2011).
[25] K. Thompson, D. Lawrence, D.J. Larson, J.D. Olson, T.F. Kelly, B. Gorman, In situ site-specific specimen preparation for atom probe tomography, Ultramicroscopy 107 (2–3) (2007) 131–139.
[26] S. Niki, P.J. Fons, A. Yamada, Y. Lacroix, H. Shibata, H. Oyanagi, M. Nishitani, T. Negami, T. Wada, Effects of the surface Cu2−xSe phase on the growth and properties of CuInSe2 films, Appl. Phys. Lett. 74 (11) (1999) 1630–1632.
[27] T. Schwarz, M.A.L. Marques, S. Botti, M. Mousel, A. Redinger, S. Siebentritt, O. Cojocaru-Mirédin, D. Raabe, P.-P. Choi, Detection of Cu2Zn5SnSe8 and Cu2Zn6SnSe9 phases in co-evaporated Cu2ZnSnSe4 thin-films, Appl. Phys. Lett. 107 (17) (2015) 172102.
[28] O.C. Hellman, J.A. Vandenbroucke, J. Rusing, D. Isheim, D.N. Seidman, Analysis of three-dimensional atom-probe data by the proximity histogram, Microsc. Microanal. Off. J. Microsc. Soc. Am. Microbeam Anal. Soc. Microsc. Soc. Can. 6 (5) (2000) 437–444.
[29] T. Schwarz, On the Nano-scale Characterization of Kesterite Thin-films, RWTH Aachen, PhD thesis, 2015.
[30] A. Redinger, S. Siebentritt, Coevaporation of Cu2ZnSnSe4 thin films, Appl. Phys. Lett. 97 (9) (2010) 092111.
[31] T. Schwarz, O. Cojocaru-Miredin, P. Choi, M. Mousel, A. Redinger, S. Siebentritt, D. Raabe, Atom probe tomography study of internal interfaces in Cu2ZnSnSe4 thin-films, J. Appl. Phys. 118 (9) (2015) 095302.
[32] S. Chen, A. Walsh, J.-H. Yang, X.G. Gong, L. Sun, P.-X. Yang, J.-H. Chu, S.-H. Wei, Compositional dependence of structural and electronic properties of Cu2ZnSn(S,Se)4 alloys for thin film solar cells, Phys. Rev. B 83 (12) (2011).
[33] S. Fiechter, M. Martinez, G. Schmidt, W. Henrion, Y. Tomm, Phase relations and optical properties of semiconducting ternary sulfides in the system Cu–Sn–S, J. Phys. Chem. Solids 64 (9–10) (2003) 1859–1862.
[34] U. Rau, J.H. Werner, Radiative efficiency limits of solar cells with lateral band-gap fluctuations, Appl. Phys. Lett. 84 (19) (2004) 3735.
[35] G. Marcano, C. Rincón, L.M. de Chalbaud, D.B. Bracho, G.S. Pérez, Crystal growth and structure, electrical, and optical characterization of the

semiconductor Cu2SnSe3, J. Appl. Phys. 90 (4) (2001) 1847–1853.
[36] T. Nomura, T. Maeda, K. Takei, M. Morihama, T. Wada, Crystal structures and band-gap energies of Cu2Sn(S,Se)3 ($0 \leq x \leq 1.0$) solid solution, Phys. Status Solidi C. 10 (7–8) (2013) 1093–1097.
[37] Y.-T. Zhai, S. Chen, J.-H. Yang, H.-J. Xiang, X.-G. Gong, A. Walsh, J. Kang, S.-H. Wei, Structural diversity and electronic properties of Cu2SnX3 (X=S, Se): a first-principles investigation, Phys. Rev. B 84 (7) (2011) 075213.
[38] R. Scheer, H.W. Schock, Chalcogenide Photovoltaics: Physics, Technologies, and Thin Film Devices, Wiley-VCH Verlag GmbH & Co. KGaA, Weinheim, 2011.
[39] D. Abou-Ras, T. Kirchartz, U. Rau, Advanced Characterization Techniques for Thin Film Solar Cells, second ed., Wiley-VCH Verlag GmbH & Co. KGaA, Weinheim, 2016 (Chapter 14).